WIDE AREA DEFORMATION MAP GENERATION WITH TERRASAR-X DATA: THE TOHOKU-OKI EARTHQUAKE 2011 CASE

Nestor Yague-Martinez[(1)], Michael Eineder[(2)], Christian Minet[(2)], Birgitt Schättler[(2)]

[(1)]Starlab Barcelona SL, Teodor Roviralta 45, 08022 Barcelona, Spain. Nestor.Yague@starlab.es
[(2)]DLR, Münchnerstrasse 20, 82234 Wessling, Germany. {Michael.Eineder, Christian.Minet, Birgitt.Schaettler}@dlr.de

ABSTRACT

The German TerraSAR-X satellite, launched in 2007, acquires high resolution SAR data at X-band. Every scene acquired in Stripmap mode covers an area of ca. 30km x 50km, which is too small to study wide area deformation phenomena. In this paper the authors propose a way to overcome the limitation of the TerraSAR-X image dimensions by acquiring data spread over the whole area of interest. The Tohoku-Oki earthquake has been taken as case study.

A total of nine interferometric co-seismic pairs in Stripmap mode have been acquired distributed over the Japanese archipelago with different geometries. Cross-correlation technique has been used to derive absolute displacements in slant-range and azimuth directions for every scene. A quality assessment of the displacement maps has to be performed carefully due to the quite large time span between pre- and post-seismic acquisitions (ranging 2 to 6 months). The displacement maps are also corrected for solid earth tides and atmospheric path delays.

1. The Tohoku-Oki earthquake

Japan was struck by a M9.0 undersea megathrust earthquake on March the 11th, 2011 at 05:46 UTC. The epicenter was situated at the coordinates 38.322ºN, 142.369ºE (approximately 72 km east of the Oshika Peninsula of Tohoku) and the hypocenter was at a depth of ca. 32 km. The whole archipelago has been affected, according to GPS measurements. Disastrous tsunami waves were triggered by the event.

2. Methodology

The method is outlined in Fig. 1. Cross-correlation is performed with image patches distributed over the TerraSAR-X SSC (Single Look Slant Range Complex) pairs. This technique allows measuring local shifts between master and slave SSCs in both, slant range and azimuth directions with high precision. Since the images are taken from different positions in space, the topography produces an additional range shift (parallax). A geometric prediction is carried out to correct for these additional shifts. TerraSAR-X precise orbit state vectors and an external DEM (Digital Elevation Model) are used. Differential atmospheric path delay [4] and Solid Earth tides [3] effects are taken into account to finally obtain a displacement map. Afterwards a wide area deformation map is generated.

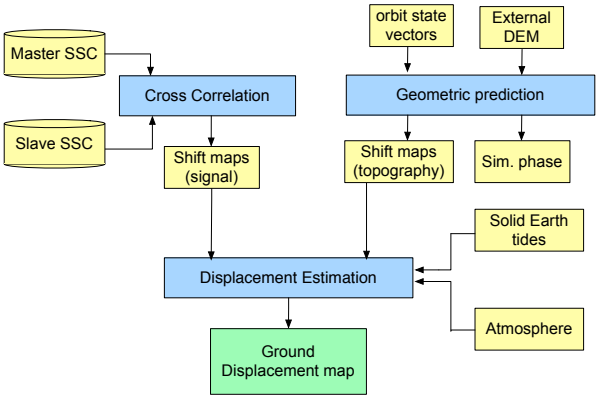

Figure 1. Methodology block diagram

2.1. Image correlation technique

Cross-correlation is applied on patches distributed regularly over the complex images. Information of both, amplitude and phase could have been used to compute correlation after the corresponding phase compensation due to parallax and topography. However, due to the quite large time span between acquisitions of our data set (see section 3.) and the large ground displacements, the phase is highly decorrelated, thus coherent cross-correlation is not possible. Pixel intensities for the correlation have been used instead. An oversampling of the complex data has been done prior the detection in order to avoid aliasing. Tab. 1 summarizes the parameters of correlation. Patches of 128x128 pixels (~190m x 250m) separated by 64 pixels (~100m) have been used. This means that a 50% patches overlap has been achieved.

A post-processing stage is applied to eliminate unreliable estimates (outliers rejection).

2.2. Atmospheric path delay correction

The atmospheric path delay has been estimated on each SAR image by using ECMWF (European Centre for Medium-Range Weather Forecasts) numerical weather

Proc. 'Fringe 2011 Workshop', Frascati, Italy,
19–23 September 2011 (ESA SP-697, January 2012)

model data. A correction for the atmospheric path delay difference has been performed on each interferometric pair. The method for the atmospheric path delay estimation is out of the scope of this paper and will not be described. Details can be found in [4].

2.3. **Solid Earth tide corrections**

The gravitational forces exerted by the Moon and the Sun produces a deformation of the Earth's crust. The height variation can reach up to 40 cm for the radial component and several centimeters for the horizontal components [3].

The slant range contribution in the radar Line of Sight (LOS) direction can be approximated using following expression [3]:

$$\delta_{ground} = -\delta_{Up} cos\theta + \delta_{East} sin\theta cos\beta - \delta_{North} sin\theta sin\beta$$

where θ is the radar looking angle and β is the heading angle i.e. the clockwise angle between the north and the ground track of the beam.

3. **TerraSAR-X dataset**

Nine descending co-seismic pairs have been acquired distributed over the archipelago with different looking angles. Every scene has been acquired in Stripmap mode and covers an area of ca. 30km x 50km. Unfortunately, there is no crossed orbit data, and thus it is not possible to derive 3D deformation maps. However, it is known from the GPS co-seismic measurements by GEONET [5] that the vertical displacements are by a factor of 6 smaller than the horizontal displacements. Taking advantage of this fact, a projection on the ground of the measured slant range displacements has been applied.

	Post-seismic scene acquisition time	Cycles	Look angle
Site 1	24.03.2011; 20:24:20	11	42.86º
Site 2	24.03.2011; 20:24:35	11	42.87º
Site 3	18.03.2011; 20:33:03	12	39.27º
Site 4	12.03.2011; 20:43:07	13	37.34º
Site 5	17.03.2011; 20:51:41	13	21.56º
Site 6	12.03.2011; 20:43:52	5	42.84º
Site 7	02.04.2011; 21:01:12	11	31.08º
Site 8	28.03.2011; 09:17:45	14	26.48º
Site 9	01.04.2011; 21:19:18	10	39.22º

Table 1. TerraSAR-X acquisitions parameters. Every cycle represents 11 days.

In Tab. 1 the TerraSAR-X acquisition times after the main earthquake, the temporal baselines in cycles (every cycle represents 11 days) and the looking angles for every site are detailed. Fig. 2 shows the geographical location of every site.

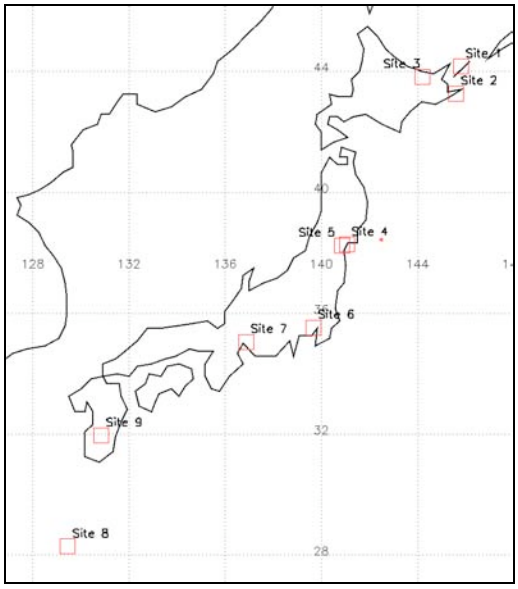

Figure 2. Geographical location of the TerraSAR-X acquisitions

In the following two subsections the acquisitions over Sendai and Tokyo will be analyzed. Then, a comparison between dInSAR (differential radar interferometry) and correlation results will be done. Finally, the wide area deformation map will be presented.

3.1. **Sendai**

Fig. 4 shows an overlay of the differential interferometric phase over the SAR amplitude (low coherence areas). Note that the interferogram suffers of high temporal decorrelation (11 cycles = 121 days temporal baseline). Nevertheless, the urban area presents good coherence. The effective baseline is 48.05m, and a multilooking of 11 x 11 pixels has been applied. A relative displacement in LOS of ca. 17cm can be measured along the plotted arrow.

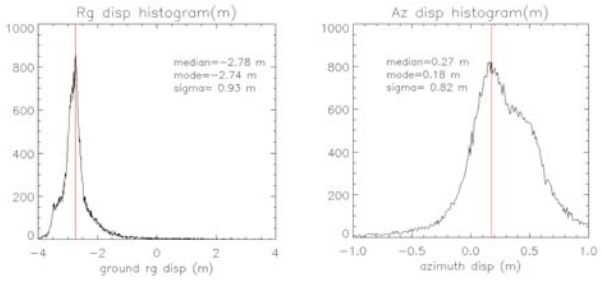

Figure 3. Histograms of the measured displacements (from cross-correlation) in range direction, projected on ground (left) and azimuth direction (right).

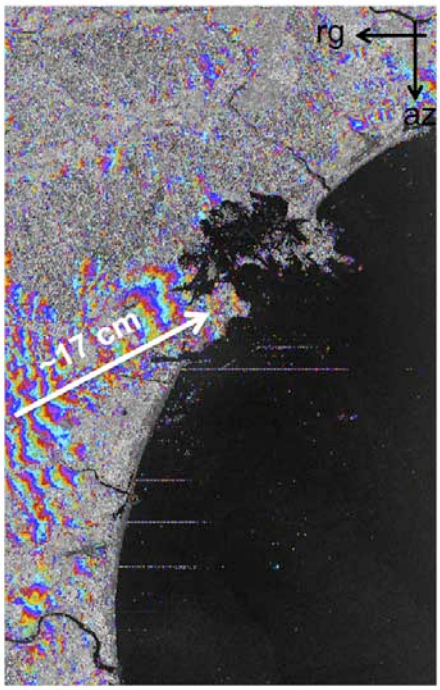

Figure 4. Overlay of the interferometric phase after topography compensation over the SAR amplitude

Fig. 5 presents an overlay of the arrow displacement map over the SAR amplitude. Every arrow averages 16x16 correlation estimates in order to get a more accurate and robust estimate. Note that this would be in the best case, because, as mentioned in section 2.1 an outlier rejection procedure has been carried out.

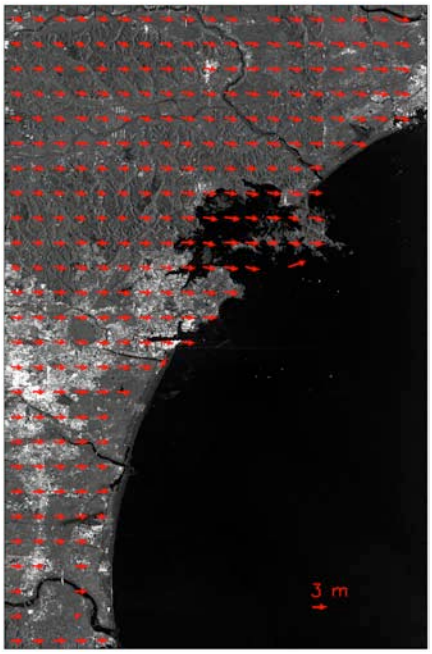

Figure 5. Arrow displacement map over SAR Amplitude

Fig. 3 shows the histograms of the measured displacements with the correlation technique in range direction, projected on ground and azimuth directions. These histograms already include the atmospheric path delay and Solid Earth tides corrections. The red line represents the mode of the histogram and will be taken as the representative displacement value of every scene for the wide area displacement map generation.

Fig. 6 shows the differential atmospheric path delay map in slant range direction between both acquisitions. Its corresponding histogram is shown in Fig. 7. A mean value of -15.4cm has been corrected.

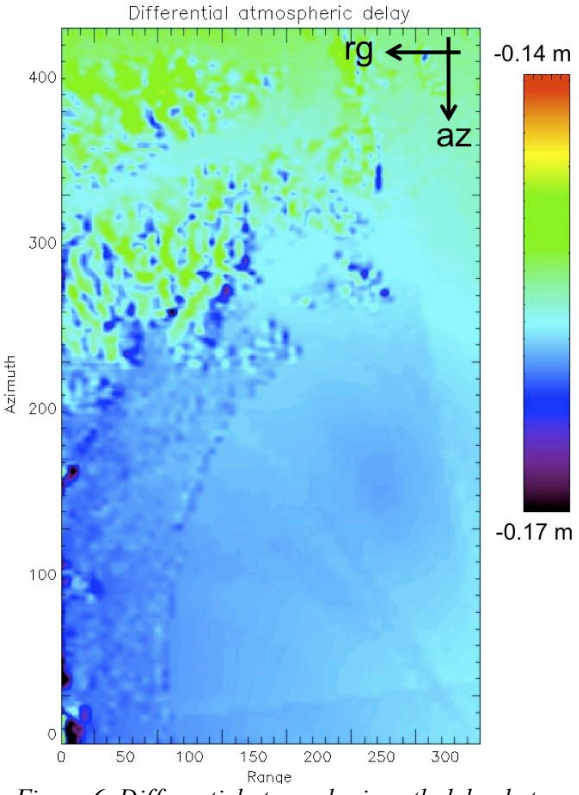

Figure 6. Differential atmospheric path delay between the acquisitions on 23.11.2010 and on 12.03.2011

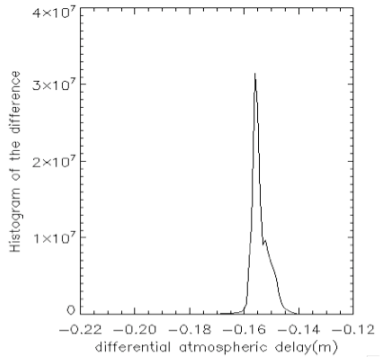

Figure 7. Histogram of the differential atmospheric path delay between both acquisition dates

The deformation values in vertical and horizontal displacements due to the Solid Earth tides are detailed in Tab. 2. The mean applied correction in the radar LOS is ca. 2.5cm.

	North	East	Up
23.11.2010	-0.88 cm	2.09 cm	-11.09 cm
12.03.2011	-3.64 cm	-0.35 cm	-7.49 cm
Difference	-2.76 cm	-2.44 cm	4.50 cm

Table 2. Solid Earth tides correction for Tokyo acquisitions.

3.2. **Tokyo**

Fig. 8 shows the interferometric phase after topographic phase compensation. This interferogram presents a better coherence than the previous one due to the shorter temporal baseline (2 months). The effective baseline is 116.36m. A multilooking of 11x11 has been applied. A relative displacement in LOS direction of ca. 11cm can be measured from late to early azimuth.

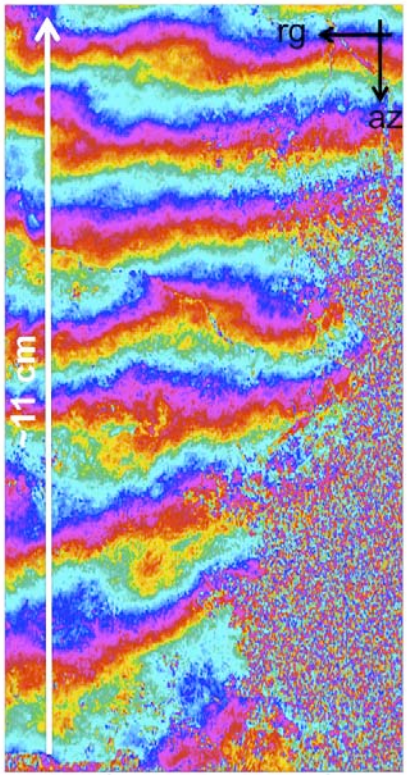

Figure 8. Interferometric phase after topographic compensation.

Fig. 9 shows the overlay of the arrow displacement map over the SAR amplitude. As for the Sendai case, every arrow is the average of 16x16 correlation estimates.

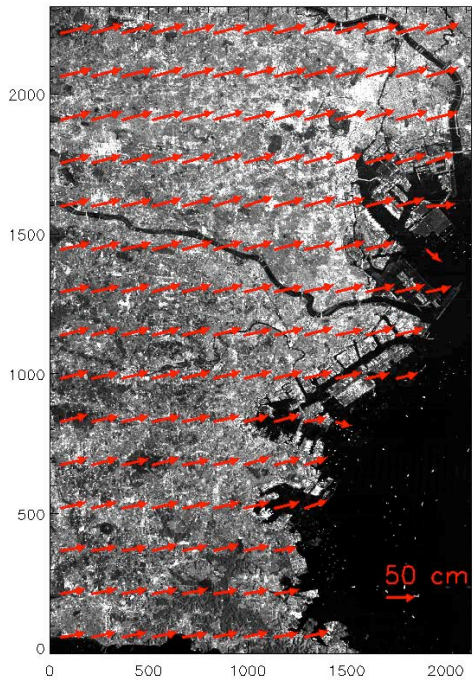

Figure 9. Arrow displacement map over SAR Amplitude

3.3. **Comparison between dInSAR and correlation techniques**

In this section, a cross comparison between both techniques, dInSAR and cross-correlation, will be done. The Tokyo interferogram has been taken as example. From the differential interferogram of Fig. 8, it can be seen that a fringe pattern over azimuth appears. That means that the LOS displacements are ca. 11cm larger in early azimuth than in late azimuth. Fig. 11 shows the profiles of the LOS displacements derived respectively from the differential phase (in black) and from the cross-correlation estimates (in red). For visualization purposes, the absolute displacement has been added to the displacements derived from the interferometric phase using information from cross-correlation.

As mentioned before, the phase has been multilooked with 11x11 looks. Additionally 50 columns have been averaged over range.

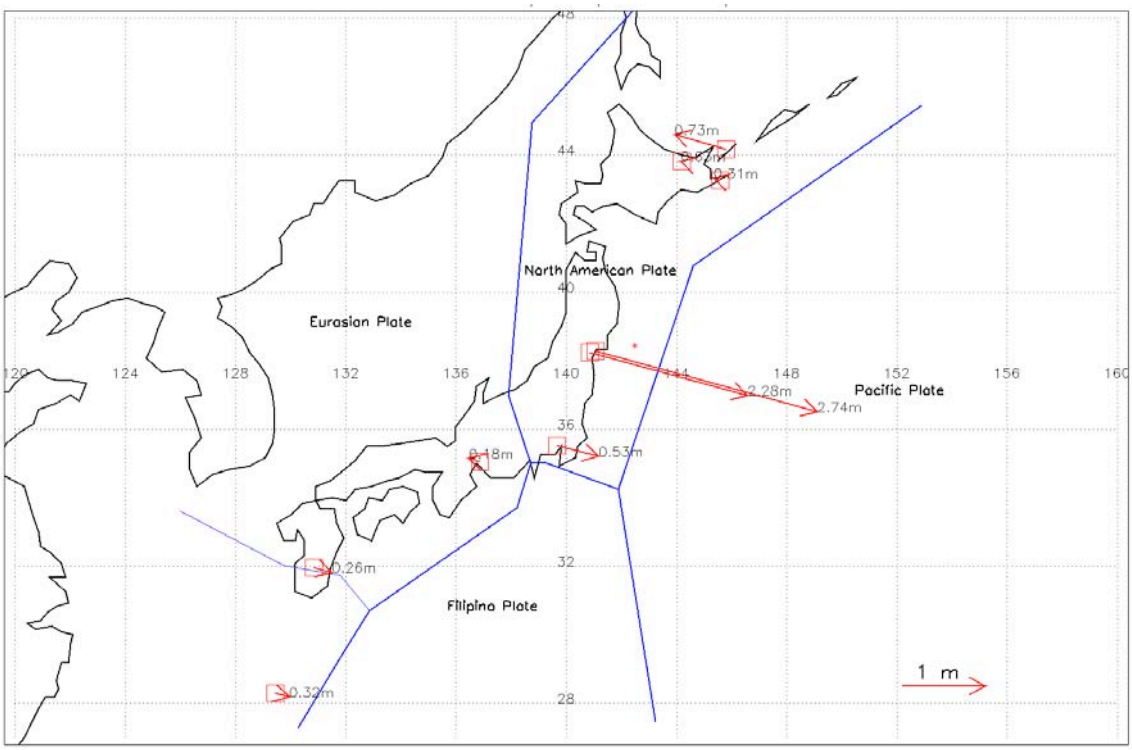

Figure 10.TerraSAR-X displacement map.

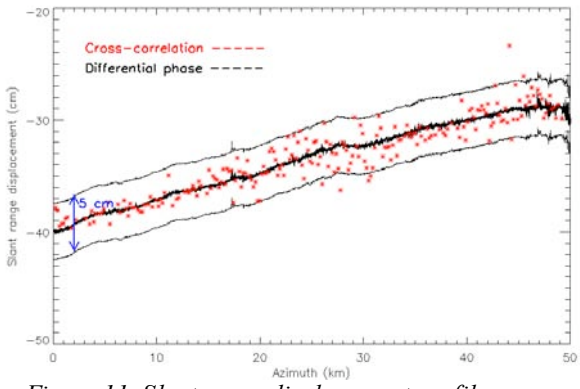

Figure 11. Slant range displacement profile over azimuth.

3.4. **Wide Area Deformation map**

Fig. 10 shows the wide area displacement map obtained combining several TerraSAR-X images. A single arrow indicating displacement amplitude and direction has been assigned to every site. The statistical modes of the range and azimuth displacement histograms have been used for this purpose (represented by the red line in Fig. 3). Fig. 12 shows the co-seismic displacement map from GPS. A qualitative agreement can be seen for the sites covered by the GPS map. A quantitative comparison will be done, when the GPS data are available to us. The displacement derived from TerraSAR-X for the site 6 (acquisition over Tokyo, Fig. 2) does not agree with the co-seismic GPS displacement. We found a possible explanation for this: the post-seismic acquisition over Tokyo took place on March the 12th at 20:43 UTC, approximately 39 hours after the main shock. In Fig. 13 the GPS first 8 hours of post-seismic displacement map [7] is shown. It can be seen that there is activity in Tokyo area, and then the aftershocks could be responsible for this displacement. We are further investigating this hypothesis.

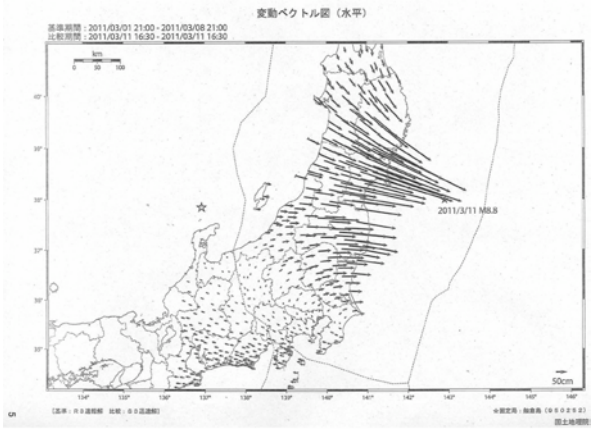

Figure 12. Co-seismic displacement map from GPS by GEONET. Acknowledgement: Prof. Hashimoto[6].

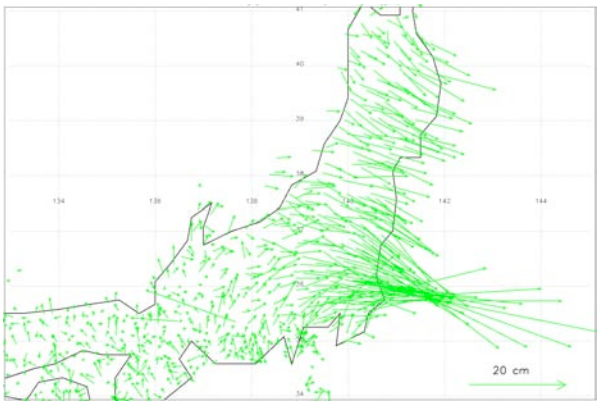

Figure 13. GPS early post-seismic displacement map Acknowledgement: ARIA team at JPL and Caltech. All Original GEONET RINEX data provided to Caltech by the Geospatial Information Authority (GSI) of Japan.

4. Conclusions

We have shown that using multiple scenes of TerraSAR-X large area displacement maps can be generated that compare well with GPS derived maps. From other experiments [3] we expect line of sights accuracies on the order of 3 to 5 centimeters. Currently our analysis is based on one-dimensional comparison but this can be extended by combining image pairs from ascending and descending passes. A quantitative comparison will be done as soon as the GPS data are available to us.

5. Acknowledgements

The authors thank X. Cong from DLR for the atmospheric path delay corrections. Thanks also to the Tohoku supersite [6], and especially to Professor Hashimoto from Kyoto University for providing the co-seismic GPS displacement map and to ARIA team at JPL and Caltech and Geospatial Information Authority of Japan for providing the early post-seismic GPS displacements map.

6. References

[1] S. Ozawa, T. Nishimura, H. Suito, T. Kobayashi, M. Tobita, T. Imakiire. Coseismic and postseismic slip of the 2011 magnitude-9 Tohoku-Oki earthquake. Letter Nature. 21 July 2011, vol 475, pp. 373 - 377

[2] R. Bamler, M. Eineder. Accuracy of Differential Shift Estimation by Correlation and Split-Bandwidth Interferometry for Wideband and Delta-k SAR Systems. IEEE Geoscience and Remote Sensing Letters. vol 2. no. 2. April 2005.

[3] M. Eineder, C. Minet, P. Steigenberger, X. Cong, T. Fritz. Imaging Geodesy – Toward Centimeter-level Ranging Accuracy with TerraSAR-X. IEEE Transactions on Geoscience and Remote Sensing, vol 49, no 2. February 2011

[4] X. Cong, M. Eineder, R. Brcic, N. Adam, C. Minet. Validation of Centimeter-Level SAR Geolocation Accuracy after Correction for Atmospheric Delay using ECMWF Weather Data. FRINGE 2011 Conference.

[5] ARIA preliminary co-seismic Displacements (vertical and horizontal displacements) from Mw9.0 Sendai-Oki Earthquake.
http://supersites.earthobservations.org/sendai.php

[6] Co-seismic displacement from GPS by GEONET. Prof. Hashimoto.
http://supersites.earthobservations.org/sendai.php

[7] Early post-seismic displacements from GPS. Provided by the ARIA team at JPL and Caltech. Original GEONET RINEX data provided to Caltech by the Geospatial Information Authority (GSI) of Japan.
http://supersites.earthobservations.org/sendai.php